Pair potentials for a metal–ceramic interface by inversion of adhesive energy

2005 J. Phys.: Condens. Matter 17 2045

(http://iopscience.iop.org/0953-8984/17/12/025)

INSTITUTE OF PHYSICS PUBLISHING JOURNAL OF PHYSICS: CONDENSED MATTER

J. Phys.: Condens. Matter **17** (2005) 2045–2058 doi:10.1088/0953-8984/17/12/025

Pair potentials for a metal–ceramic interface by inversion of adhesive energy

Y Long[1], **N X Chen**[1,2] **and W Q Zhang**[3]

[1] Department of Physics, Tsinghua University, Beijing 100084, People's Republic of China
[2] Institute for Applied Physics, University of Science and Technology, 100083, People's Republic of China
[3] Shanghai Institute of Ceramics, Chinese Academy of Sciences, 200050, People's Republic of China

E-mail: longyao@tsinghua.org.cn

Received 12 January 2005, in final form 22 February 2005
Published 11 March 2005
Online at stacks.iop.org/JPhysCM/17/2045

Abstract

A concise and general formula is introduced to obtain *ab initio* pair potentials between atoms across a metal–ceramic interface by inversion of the adhesive energies of the interface. Derivation of interfacial potentials Φ_{Ag-Mg} and Φ_{Ag-O} from *ab initio* adhesive energies is performed by applying the formula to the Ag/MgO(001) interface. Transferability of these potentials at Ag/MgO(100), Ag/MgO(110) and Ag/MgO(111) interfaces is discussed.

1. Introduction

Metal–ceramic interfaces have attracted considerable attention in both experimental and theoretical research due to their extensive applications to catalytic converters, field effect transistors, anticorrosion coatings and composite materials. Experimentally, advanced technologies such as grazing incidence x-ray scattering (GIXS) [1–3] and high resolution transmission electron microscopy (HRTEM) [4–8] have been applied to structure observation of atomistic scale, and many features of different interfaces have been revealed. However, there are still a lot of problems remaining for the measurement and characterization of complex interfaces. In addition, no current theoretical method can provide a complete description of interface configurations since so many possible metastable structures exist for a real interface system. From this point of view, a reliable and efficient computational method is really necessary for research on interface.

Two types of computational approach are normally adopted for theoretical interface studies: *ab initio* calculation [9–13] and atomistic simulation [14–17]. The *ab initio* approach is reliable but very time-consuming. It can be used only for a small model system with several hundreds of atoms. The atomistic simulation based on interatomic potentials is efficient. It can be applied to a large system with thousands of atoms, provided interatomic potentials can

be obtained in a systematic and reliable way. Therefore, a valid way of extracting reliable interatomic potentials is of great help to interface research.

Many methods have been developed for the derivation of atomic potentials for bulk materials such as the shell model, embedded-atom model, and environment dependent potentials [18–20], etc. For interfaces, due to the complicated arrangement of atoms at interfaces, few methods have been proposed to obtain reliable potentials. Some interesting works along this line for metal–ceramic interfaces are the discrete classical model (DCM) from Duffy [15], Finnis [14] and Purton *et al* [16, 17], and the *ab initio* approach from Endou [21] and Yao [22]. In addition, the Green function method has been applied in the investigation of interfaces by Moliner [23] and Quintanar [24] through tight binding studies. The DCM cannot reproduce the adhesive energies very well, and Yao's iteration method is a little too complex for calculation and analysis, since too many infinite summations are involved.

In this paper, we introduce a method to obtain interatomic pair potentials between atoms across an interface by inversion of the *ab initio* adhesive energy curves of the interface. The method is based on a number theory, called the Mobius inversion method, proposed by one of the authors in the 1990s [25, 26]. It has been applied to obtain reliable interatomic potentials for many bulk materials successfully, such as ion crystals [27], rare earth compounds [28] and semiconductors [29], and is further developed to obtain interatomic potentials for application to interfaces. As shown later, the inverse technique used for the interfacial system is based on an additive semigroup instead of a multiplicative semigroup for bulk systems.

A Ag/MgO interface is chosen as the model system for several reasons. Firstly, both parts of the interface have simple structures, with magnesium oxide of B1 and silver of fcc crystal structures. Secondly, interface mismatch, defined as

$$\frac{a_{\mathrm{MgO}} - a_{\mathrm{Ag}}}{(a_{\mathrm{MgO}} + a_{\mathrm{Ag}})/2} \tag{1}$$

amounts to only 3%, a relatively small value, and where a_{Ag} and a_{MgO} are the lattice constants of bulk Ag and MgO, respectively. Finally, the interface was observed to be atomic sharp with silver atoms being at the epitaxial positions relative to MgO(001) surface [1, 3]. For these reasons, the Ag/MgO interface has been widely studied over the past few years [1–3, 5, 7, 8]. The mode of epitaxy growth, interface distance, wetting angle and adsorption sites for Ag atoms on a MgO(001) surface were investigated carefully [1, 3, 5]. *Ab initio* computations of the structure and adhesion of the interface were also performed by the linearized muffin tin orbitals (LMTO) method [10, 11], local-density approximation (LDA) [12] and generalized gradient approximation (GGA) [13]. Therefore, this work has a special advantage due to the existence of many references for comparison.

2. Methodology

Now let us show how to extract interatomic potentials between atoms across the Ag/MgO(001) interface from the *ab initio* adhesive energies. The method is built on an assumption that the adhesive energy of an interface can be expressed as the summation over all pair interactions between atoms across the interface. This is obviously a rough approximation because of the complexity of chemical bonds at a real metal–ceramic interface. However, we show that such a pair potential approach gives a reasonable description of the complex interfacial structures to some extent. This is not really a surprise to us because, as a matter of fact, the pair potential approach has been used widely to study complex materials phenomena [28], including interfaces (DCM [14–17] and Kohyama–Morse [30, 31]), and many good results were obtained.

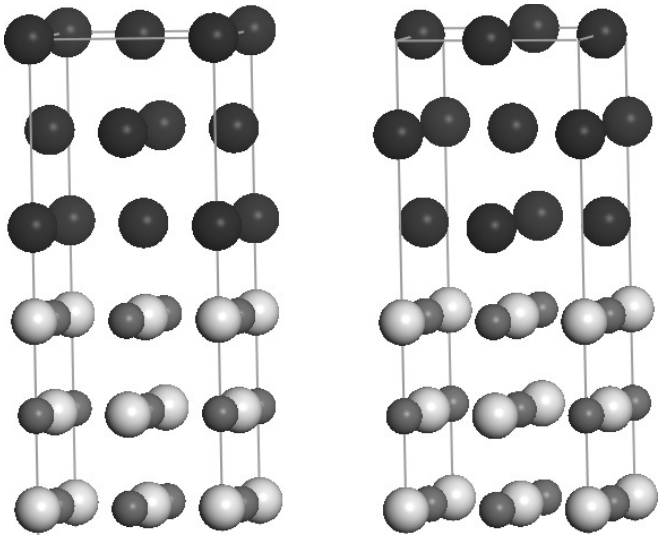

Figure 1. Interface structures of Ag/MgO(001). Left: Ag on Mg. Right: Ag on O. Black spheres represent silver, light grey spheres represent magnesium and dark grey spheres represent oxygen.

There are basically two types of pair potential, $\Phi_{\mathrm{Ag-Mg}}$ for Ag–Mg and $\Phi_{\mathrm{Ag-O}}$ for Ag–O interactions, across the Ag/MgO(001) interface. Therefore, the adhesive energy of the Ag/MgO interface can be expressed as:

$$E_{\mathrm{ad}} = \sum_{i,j} \Phi_{\mathrm{Ag-Mg}}(r_{i,j}) + \sum_{i',j'} \Phi_{\mathrm{Ag-O}}(r_{i',j'}) \tag{2}$$

where i', j' represent the Ag–Mg (Ag–O) pairs, and r is the distance between the corresponding Ag and Mg (Ag and O) atoms.

Adhesive energy curves for two different interfacial configurations, with Ag atoms atop of Mg or O sites separately (see figure 1), have to be obtained from *ab initio* calculations (see below for computational details) in order to extract potentials $\Phi_{\mathrm{Ag-Mg}}$ and $\Phi_{\mathrm{Ag-O}}$. Let x be the interfacial distance of the Ag/MgO system, and a be the lattice constants of crystals Ag and MgO, which have been forced to have the same lattice constant in order to form an commensurate interface. Denoting the adhesive energy curves of the two interfacial configurations as $E_{\mathrm{Mg}}(x)$ for Ag atop of Mg sites and $E_{\mathrm{O}}(x)$ for Ag atop of O sites (see figure 1), they can be expressed as:

$$\begin{aligned}
E_{\mathrm{Mg}}(x) = \sum_{l,l'=0}^{\infty} \sum_{m,n=-\infty}^{\infty} \Bigg\{ & \Phi_{\mathrm{Ag-Mg}}\left(\sqrt{(x+la+l'a)^2+(ma)^2+(na)^2}\right) \\
& + \Phi_{\mathrm{Ag-Mg}}\left(\sqrt{(x+la+l'a)^2+((m+1/2)a)^2+((n+1/2)a)^2}\right) \\
& + \Phi_{\mathrm{Ag-Mg}}\left(\sqrt{(x+la+(l'+1/2)a)^2+(ma)^2+((n+1/2)a)^2}\right) \\
& + \Phi_{\mathrm{Ag-Mg}}\left(\sqrt{(x+la+(l'+1/2)a)^2+((m+1/2)a)^2+(na)^2}\right) \\
& + \Phi_{\mathrm{Ag-Mg}}\left(\sqrt{(x+(l+1/2)a+l'a)^2+(ma)^2+((n+1/2)a)^2}\right) \\
& + \Phi_{\mathrm{Ag-Mg}}\left(\sqrt{(x+(l+1/2)a+l'a)^2+((m+1/2)a)^2+(na)^2}\right)
\end{aligned}$$

$$
\begin{aligned}
&+\Phi_{\mathrm{Ag-Mg}}\left(\sqrt{(x+(l+1/2)a+(l'+1/2)a)^2+(ma)^2+(na)^2}\right)\\
&+\Phi_{\mathrm{Ag-Mg}}\left(\sqrt{(x+(l+1/2)a+(l'+1/2)a)^2+((m+1/2)a)^2+((n+1/2)a)^2}\right)\\
&+\Phi_{\mathrm{Ag-O}}\left(\sqrt{(x+la+l'a)^2+(ma)^2+((n+1/2)a)^2}\right)\\
&+\Phi_{\mathrm{Ag-O}}\left(\sqrt{(x+la+l'a)^2+((m+1/2)a)^2+(na)^2}\right)\\
&+\Phi_{\mathrm{Ag-O}}\left(\sqrt{(x+la+(l'+1/2)a)^2+(ma)^2+(na)^2}\right)\\
&+\Phi_{\mathrm{Ag-O}}\left(\sqrt{(x+la+(l'+1/2)a)^2+((m+1/2)a)^2+((n+1/2)a)^2}\right)\\
&+\Phi_{\mathrm{Ag-O}}\left(\sqrt{(x+(l+1/2)a+l'a)^2+(ma)^2+(na)^2}\right)\\
&+\Phi_{\mathrm{Ag-O}}\left(\sqrt{(x+(l+1/2)a+l'a)^2+((m+1/2)a)^2+((n+1/2)a)^2}\right)\\
&+\Phi_{\mathrm{Ag-O}}\left(\sqrt{(x+(l+1/2)a+(l'+1/2)a)^2+(ma)^2+((n+1/2)a)^2}\right)\\
&+\Phi_{\mathrm{Ag-O}}\left(\sqrt{(x+(l+1/2)a+(l'+1/2)a)^2+((m+1/2)a)^2+(na)^2}\right)\Bigg\} \qquad (3)
\end{aligned}
$$

$$
\begin{aligned}
E_{\mathrm{O}}(x)=\sum_{l,l'=0}^{\infty}\sum_{m,n=-\infty}^{\infty}\Bigg\{&\Phi_{\mathrm{Ag-O}}\left(\sqrt{(x+la+l'a)^2+(ma)^2+(na)^2}\right)\\
&+\Phi_{\mathrm{Ag-O}}\left(\sqrt{(x+la+l'a)^2+((m+1/2)a)^2+((n+1/2)a)^2}\right)\\
&+\Phi_{\mathrm{Ag-O}}\left(\sqrt{(x+la+(l'+1/2)a)^2+(ma)^2+((n+1/2)a)^2}\right)\\
&+\Phi_{\mathrm{Ag-O}}\left(\sqrt{(x+la+(l'+1/2)a)^2+((m+1/2)a)^2+(na)^2}\right)\\
&+\Phi_{\mathrm{Ag-O}}\left(\sqrt{(x+(l+1/2)a+l'a)^2+(ma)^2+((n+1/2)a)^2}\right)\\
&+\Phi_{\mathrm{Ag-O}}\left(\sqrt{(x+(l+1/2)a+l'a)^2+((m+1/2)a)^2+(na)^2}\right)\\
&+\Phi_{\mathrm{Ag-O}}\left(\sqrt{(x+(l+1/2)a+(l'+1/2)a)^2+(ma)^2+(na)^2}\right)\\
&+\Phi_{\mathrm{Ag-O}}\left(\sqrt{(x+(l+1/2)a+(l'+1/2)a)^2+((m+1/2)a)^2+((n+1/2)a)^2}\right)\\
&+\Phi_{\mathrm{Ag-Mg}}\left(\sqrt{(x+la+l'a)^2+(ma)^2+((n+1/2)a)^2}\right)\\
&+\Phi_{\mathrm{Ag-Mg}}\left(\sqrt{(x+la+l'a)^2+((m+1/2)a)^2+(na)^2}\right)\\
&+\Phi_{\mathrm{Ag-Mg}}\left(\sqrt{(x+la+(l'+1/2)a)^2+(ma)^2+(na)^2}\right)\\
&+\Phi_{\mathrm{Ag-Mg}}\left(\sqrt{(x+la+(l'+1/2)a)^2+((m+1/2)a)^2+((n+1/2)a)^2}\right)\\
&+\Phi_{\mathrm{Ag-Mg}}\left(\sqrt{(x+(l+1/2)a+l'a)^2+(ma)^2+(na)^2}\right)\\
&+\Phi_{\mathrm{Ag-Mg}}\left(\sqrt{(x+(l+1/2)a+l'a)^2+((m+1/2)a)^2+((n+1/2)a)^2}\right)\\
&+\Phi_{\mathrm{Ag-Mg}}\left(\sqrt{(x+(l+1/2)a+(l'+1/2)a)^2+(ma)^2+((n+1/2)a)^2}\right)\\
&+\Phi_{\mathrm{Ag-Mg}}\left(\sqrt{(x+(l+1/2)a+(l'+1/2)a)^2+((m+1/2)a)^2+(na)^2}\right)\Bigg\} \qquad (4)
\end{aligned}
$$

where the variables on the right-hand side indicate the distance between Ag and O or Ag and Mg. For example, $(x + la + l'a)$ is the perpendicular component to the interface plane, and $\sqrt{(ma)^2 + (na)^2}$ is the corresponding parallel component.

Deriving interfacial potentials $\Phi_{\mathrm{Ag-Mg}}(r)$ and $\Phi_{\mathrm{Ag-O}}(r)$ from adhesion curves $E_{\mathrm{Mg}}(x)$ and $E_{\mathrm{O}}(x)$ is not an easy job, because equations (3) and (4) are complex equations with cross-coupling items. Mathematical skill must be used and simplification has to be done for that purpose.

By defining

$$E_{\pm}(x) = E_{\mathrm{Mg}}(x) \pm E_{\mathrm{O}}(x) \tag{5}$$

$$\Phi_{\pm}(r) = \Phi_{\mathrm{Ag-Mg}}(r) \pm \Phi_{\mathrm{Ag-O}}(r) \tag{6}$$

we have

$$\begin{aligned}
E_{\pm}(x) = \sum_{l,l'=0}^{\infty} \sum_{m,n=-\infty}^{\infty} \Bigg\{ & \Phi_{\pm}\Big(\sqrt{(x + la + l'a)^2 + (ma)^2 + (na)^2}\Big) \\
& + \Phi_{\pm}\Big(\sqrt{(x + la + l'a)^2 + ((m + 1/2)a)^2 + ((n + 1/2)a)^2}\Big) \\
& + \Phi_{\pm}\Big(\sqrt{(x + la + (l' + 1/2)a)^2 + (ma)^2 + ((n + 1/2)a)^2}\Big) \\
& + \Phi_{\pm}\Big(\sqrt{(x + la + (l' + 1/2)a)^2 + ((m + 1/2)a)^2 + (na)^2}\Big) \\
& + \Phi_{\pm}\Big(\sqrt{(x + (l + 1/2)a + l'a)^2 + (ma)^2 + ((n + 1/2)a)^2}\Big) \\
& + \Phi_{\pm}\Big(\sqrt{(x + (l + 1/2)a + l'a)^2 + ((m + 1/2)a)^2 + (na)^2}\Big) \\
& + \Phi_{\pm}\Big(\sqrt{(x + (l + 1/2)a + (l' + 1/2)a)^2 + (ma)^2 + (na)^2}\Big) \\
& + \Phi_{\pm}\Big(\sqrt{(x + (l + 1/2)a + (l' + 1/2)a)^2 + ((m + 1/2)a)^2 + ((n + 1/2)a)^2}\Big) \\
& \pm \Phi_{\pm}\Big(\sqrt{(x + la + l'a)^2 + (ma)^2 + ((n + 1/2)a)^2}\Big) \\
& \pm \Phi_{\pm}\Big(\sqrt{(x + la + l'a)^2 + ((m + 1/2)a)^2 + (na)^2}\Big) \\
& \pm \Phi_{\pm}\Big(\sqrt{(x + la + (l' + 1/2)a)^2 + (ma)^2 + (na)^2}\Big) \\
& \pm \Phi_{\pm}\Big(\sqrt{(x + la + (l' + 1/2)a)^2 + ((m + 1/2)a)^2 + ((n + 1/2)a)^2}\Big) \\
& \pm \Phi_{\pm}\Big(\sqrt{(x + (l + 1/2)a + l'a)^2 + (ma)^2 + (na)^2}\Big) \\
& \pm \Phi_{\pm}\Big(\sqrt{(x + (l + 1/2)a + l'a)^2 + ((m + 1/2)a)^2 + ((n + 1/2)a)^2}\Big) \\
& \pm \Phi_{\pm}\Big(\sqrt{(x + (l + 1/2)a + (l' + 1/2)a)^2 + (ma)^2 + (na)^2}\Big) \\
& \pm \Phi_{\pm}\Big(\sqrt{(x + (l + 1/2)a + (l' + 1/2)a)^2 + ((m + 1/2)a)^2 + ((n + 1/2)a)^2}\Big) \Bigg\}.
\end{aligned} \tag{7}$$

In fact, equation (7) are two independent equations equivalent to equations (3) and (4). Once we are able to extract $\Phi_{\pm}(r)$ from $E_{\pm}(x)$, the interfacial potentials could be obtained by:

$$\begin{aligned}
\Phi_{\mathrm{Ag-Mg}} &= \frac{\Phi_+ + \Phi_-}{2} \\
\Phi_{\mathrm{Ag-O}} &= \frac{\Phi_+ - \Phi_-}{2}.
\end{aligned} \tag{8}$$

Obviously, the procedure for extracting $\Phi_+(r)$ or $\Phi_-(r)$ from $E_+(x)$ or $E_-(x)$ is the same. Therefore, only the route for $\Phi_+(r)$ is described in detail as follows. Also, from equation (7), $E_+(x)$ can be expressed by $\Phi_+(r)$ in a more compact way such that

$$E_+(x) = \sum_{i,j=0}^{\infty} \sum_{s,t=-\infty}^{\infty} \Phi_+\Big(\sqrt{(x + (i+j)a/2)^2 + (s^2+t^2)(a/2)^2}\Big). \tag{9}$$

For further simplification, equation (9) can be separated into two independent equations, equations (10) and (11). The first one, with a newly defined function $H_+(x)$, is

$$H_+(x) = \sum_{s,t=-\infty}^{\infty} \Phi_+\Big(\sqrt{x^2 + (s^2+t^2)(a/2)^2}\Big). \tag{10}$$

$E_+(x)$ can then be expressed by $H_+(x)$ as:

$$E_+(x) = \sum_{i,j=0}^{\infty} H_+(x + (i+j)a/2). \tag{11}$$

This is the second equation. Now let us first show how to get $H_+(x)$ from equation (11) and then $\Phi_+(r)$ from equation (10).

From equation (11), we have:

$$E_+(x) - E_+(x + a/2) = \sum_{j=0}^{\infty} H_+(x + ja/2) \tag{12}$$

and

$$E_+(x + a/2) - E_+(x + a) = \sum_{j=1}^{\infty} H_+(x + ja/2). \tag{13}$$

Therefore, it is given that:

$$\begin{aligned} H_+(x) &= (E_+(x) - E_+(x + a/2)) - (E_+(x + a/2) - E_+(x + a)) \\ &= E_x(x) - 2E_+(x + a/2) + E_+(x + a). \end{aligned} \tag{14}$$

Equation (11) is solved.

In order to solve equation (10), we rewrite it as

$$H_+(x) = \sum_{n=0}^{\infty} h(n)\Phi_+\Big(\sqrt{x^2 + n(a/2)^2}\Big) \tag{15}$$

where $h(n)$ is the coefficient, which is defined as

$$h(n) = \begin{cases} 1 & \text{if } n = 0 \\ 4 & \text{if } n = s^2 \text{ or } 2s^2 \qquad \text{with } s \neq 0 \\ 8 & \text{if } n = s^2 + t^2 \qquad \text{with } 0 \neq |s| \neq |t| \neq 0 \\ 0 & \text{if } n \neq s^2 + t^2. \end{cases} \tag{16}$$

Note that once the case of $s_1^2 + t_1^2 = n = s_2^2 + t_2^2$ with $(s_1, t_1) \neq (s_2, t_2)$ occurs, we have to consider the combination, for example, $s_1^2 + t_1^2 = n = s_2^2 + t_2^2$ with $s_1^2 = t_1^2$ and $0 \neq s_2^2 \neq t_2^2 \neq 0$, then $h(n) = 4 + 8 = 12$; a concrete example is $(s_1, t_1) = (5, 5)$ and $(s_2, t_2) = (1, 7)$.

To obtain $\Phi_+(r)$ from $H_+(x)$ based on equation (15) is an inverse problem. Now, we determine the inversion coefficients $g(n)$, which satisfies a recursive relation:

$$\sum_{m=0}^{n} h(m)g(n - m) = \delta_{n,0} \tag{17}$$

$\delta_{n,0}$ is the Kronecker function, which satisfies

$$\delta_{n,0} = \begin{cases} 1 & n = 0 \\ 0 & n \geqslant 1. \end{cases} \tag{18}$$

From equations (15) and (17), it is easy to prove that

$$\begin{aligned} \sum_{k=0}^{\infty} g(k) H_+\Big(\sqrt{x^2 + k(a/2)^2}\Big) &= \sum_{k=0}^{\infty} g(k) \sum_{m=0}^{\infty} h(m) \Phi_+\Big(\sqrt{x^2 + k(a/2)^2 + m(a/2)^2}\Big) \\ &= \sum_{n=0}^{\infty} \Big(\sum_{m=0}^{n} h(m) g(n-m) \Big) \Phi_+\Big(\sqrt{x^2 + n(a/2)^2}\Big) \\ &= \sum_{n=0}^{\infty} \delta_{n,0} \Phi_+\Big(\sqrt{x^2 + n(a/2)^2}\Big) \\ &= \Phi_+(x). \end{aligned} \tag{19}$$

Therefore, the solution of equation (15) can be written as:

$$\Phi_+(x) = \sum_{n=0}^{\infty} g(n) H_+\Big(\sqrt{x^2 + n(a/2)^2}\Big). \tag{20}$$

Combining equation (14) with equation (20), $\Phi_+(x)$ is given as

$$\begin{aligned} \Phi_+(x) = \sum_{n=0}^{\infty} g(n) \Big(& E_+\Big(\sqrt{x^2 + n(a/2)^2}\Big) - 2E_+\Big(\sqrt{x^2 + n(a/2)^2} + a\Big) \\ & + E_+\Big(\sqrt{x^2 + n(a/2)^2} + 2a\Big)\Big). \end{aligned} \tag{21}$$

In a similar way, $\Phi_-(x)$ can be derived from $E_-(x)$. The final solution of equations (3) and (4) can be obtained from equation (8). Note that the above inversion procedure is suitable not only for the Ag/MgO(001) interface, but also for many similar systems, such as Pd/MgO, Cu/MgO, V/MgO and Fe/MgO. To be consistent with our early works for bulk materials [25–29], this is called the Mobius inversion method.

Note that the inversion coefficient $g(n)$ for the interfacial potential is given by an additive recursive relation as

$$\sum_{m=0}^{n} h(m) g(n-m) = \delta_{n,0}$$

and the inversion coefficient $g(n)$ for the bulk material potential is given by a multiplicative recursive relation as

$$\sum_{m|n} h(m) g(n/m) = \delta_{n1};$$

the former corresponds to the Mobius inversion on additive semi-group, and the latter corresponds to that on multiplicative semi-group.

3. Results

Ab initio computation is performed by CASTEP [32, 33] using a ultrasoft pseudopotential with the generalized gradient approximation (GGA). The kinetic energy cutoff is 340 eV. The k-points are generated using the Monkhorst–Pack scheme, with the parameters (11 11 2) [34, 35]. There are 21 k-points in the reduced Brillouin zone.

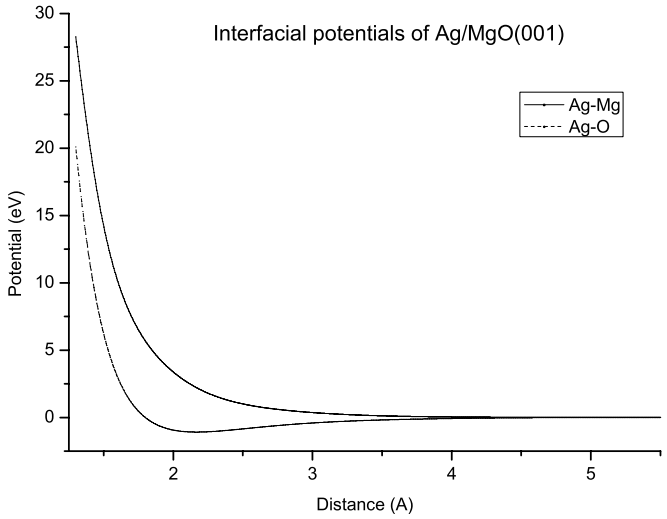

Figure 2. Potential curves of Ag/MgO(001). The solid curve represents Ag–Mg, the dashed curve represents Ag–O.

Table 1. Parameters of pair potentials across the Ag/MgO(001) interface.

Atom pair	Potential parameters		
Ag–Mg	$D_0 = 284.5542$ kcal mol^{-1}	$R_0 = 1$ Å	$y = 2.0843$
	$a_1 = 1600.6582$ kcal mol^{-1}	$b_1 = 6.2388$ Å^{-1}	$c_1 = 1.1478$ Å
	$a_2 = 7.0657$ kcal mol^{-1}	$b_2 = 3.6581$ Å^{-1}	$c_2 = 2.9842$ Å
	$a_3 = 71.1797$ kcal mol^{-1}	$b_3 = 4.3778$ Å^{-1}	$c_3 = 1.8999$ Å
Ag–O	$D_0 = 5596.5601$ kcal mol^{-1}	$R_0 = 1$ Å	$y = 2.1383$
	$a_1 = -5678.4394$ kcal mol^{-1}	$b_1 = 2.8384$ Å^{-1}	$c_1 = 1.0839$ Å
	$a_2 = -634.8887$ kcal mol^{-1}	$b_2 = 2.1121$ Å^{-1}	$c_2 = 1.9$ Å
	$a_3 = -7.4067$ kcal mol^{-1}	$b_3 = 2.5757$ Å^{-1}	$c_3 = 3.5539$ Å

In order to obtain the *ab initio* adhesive energies, the interface distance range (figure 1) varies from 1.5 to 5.0 Å. The converted interfacial potentials are then given through the method discussed in section 2, and fit into the modified Rahman–Stillinger–Lemberg potential (RSL2):

$$E = D_0 \mathrm{e}^{y(1-\frac{R}{R_0})} + \frac{a_1}{1+\mathrm{e}^{b_1(R-c_1)}} + \frac{a_1}{1+\mathrm{e}^{b_2(R-c_2)}} + \frac{a_3}{1+\mathrm{e}^{b_3(R-c_3)}}. \tag{22}$$

The calculated parameters are presented in table 1, and potential curves are shown in figure 2.

As the potentials have been obtained, a countercheck is necessary. The *ab initio* adhesive energy curves are compared with the ones generated from potentials by equations (3) and (4), as shown in figure 3. The good agreement shows that our inversion is successful to this extent.

Now we consider the applicability of the above interfacial potentials to some other structures of Ag/MgO(001) interface. As shown in figure 4, Ag atoms are located in the middle of the Mg–Mg bond, the middle of the Mg–O bond, and at a quarter of the Mg–Mg bond. The energy curves generated by *ab initio* calculation and above interfacial potentials are presented in figure 5. We see that most of the *ab initio* curves can be exactly reproduced by potentials. Only some difference is found when Ag is located in the middle of the Mg–Mg bond. This reveals that our potentials can reproduce the energy surface of Ag/MgO(001) to a great extent.

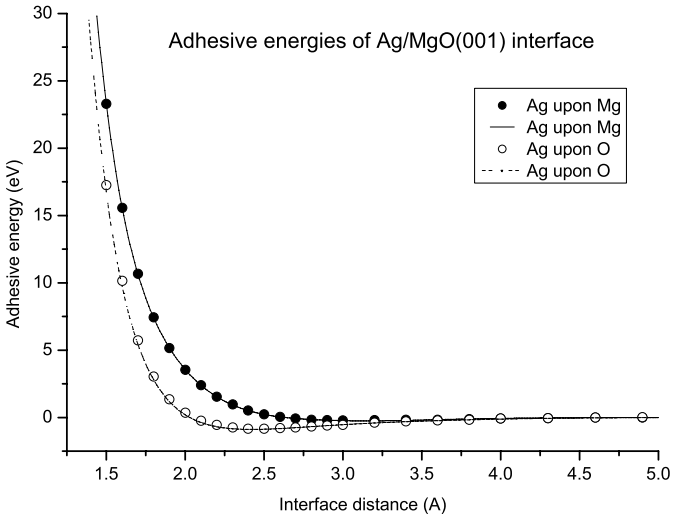

Figure 3. Adhesive energy curves from *ab initio* calculation and summation of potentials for Ag/MgO(001). Circles represent the *ab initio* results, and curves represent the summation of potentials.

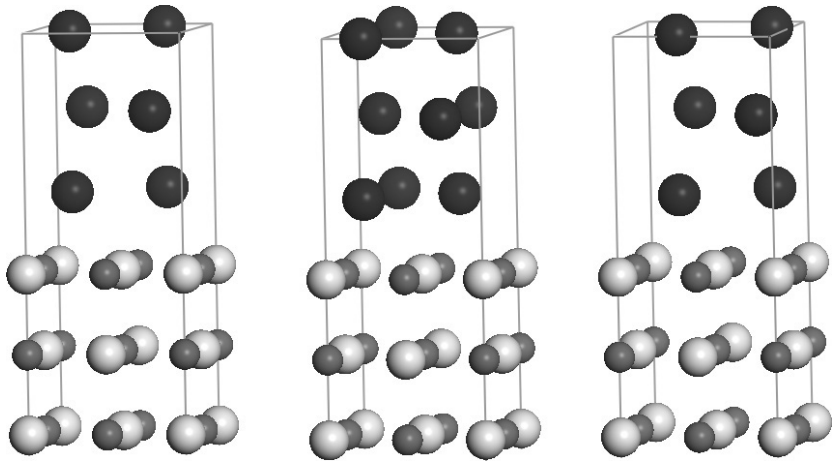

Figure 4. Interface structures of Ag/MgO(001). Left: Ag in the middle of the Mg–Mg bond. Middle: Ag in the middle of the Mg–O bond. Right: Ag at a quarter of the Mg–Mg bond. Black spheres represent silver, light grey spheres represent magnesium and dark grey spheres represent oxygen.

Next, we investigate the transferability of these interfacial potentials to interfaces Ag/MgO(110) and Ag/MgO(111). The corresponding interface structures are shown in figures 6 and 7, and the energy curves are presented in figures 8 and 9.

From the figures, the *ab initio* adhesive energy curves of the Ag/MgO(110) and Ag/MgO(111) interfaces with lowest energy structures can be reproduced by these pair potentials derived from Ag/MgO(001), but the adhesive energy curves with highest energy structures cannot be reproduced, especially for the polarized Ag/MgO(111) interface with high energy, as in figures 9(a) and (b). This is because of the transformation of the electronic

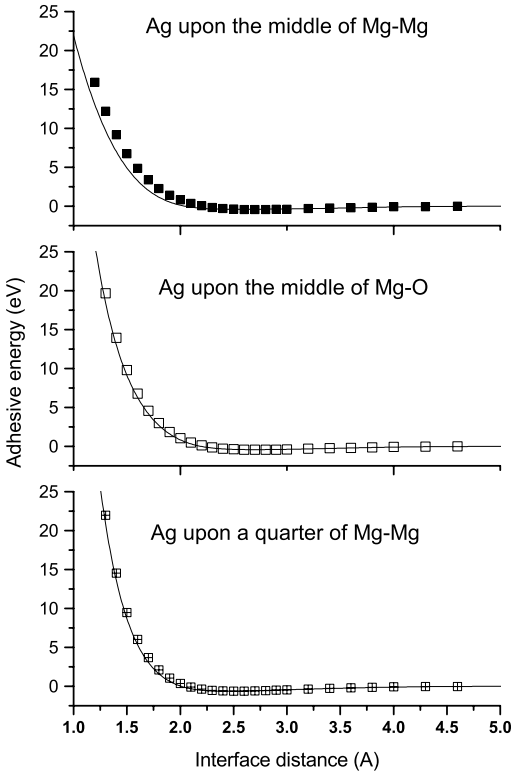

Figure 5. Adhesive energy curves from *ab initio* calculation and summation of potentials for Ag/MgO(001). Squares represent the *ab initio* results, and curves represent the summation of potentials.

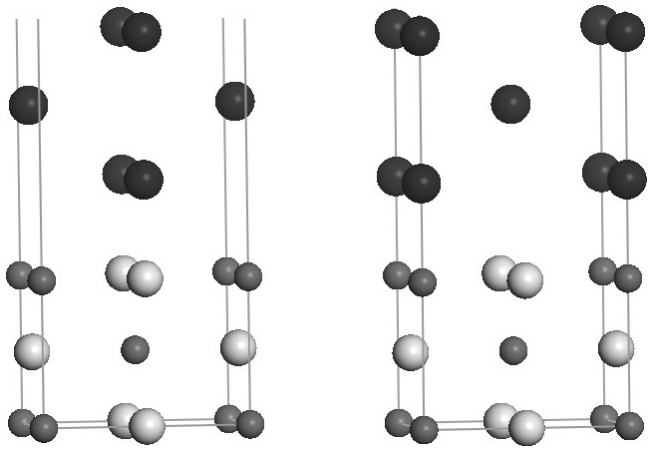

Figure 6. Interface structures of Ag/MgO(110). Left: Ag on O. Right: Ag on Mg. Black spheres represent silver, light grey spheres represent magnesium and dark grey spheres represent oxygen.

structures, as shown in figure 10. The interfaces of different Miller indices contain different charge distribution, and then produce different interfacial potentials. Fortunately, the interfacial structures with low energies can be reproduced with our potentials.

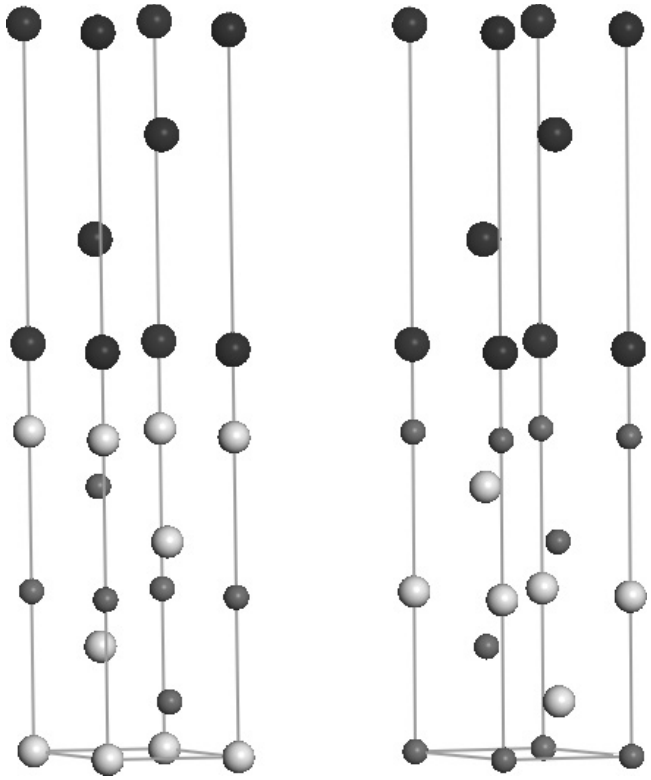

Figure 7. Interface structures of Ag/MgO(111). Left: Ag on the O terminated MgO(111) surface. Right: Ag on the Mg terminated MgO(111) surface. Black spheres represent silver, light grey spheres represent magnesium and dark grey spheres represent oxygen.

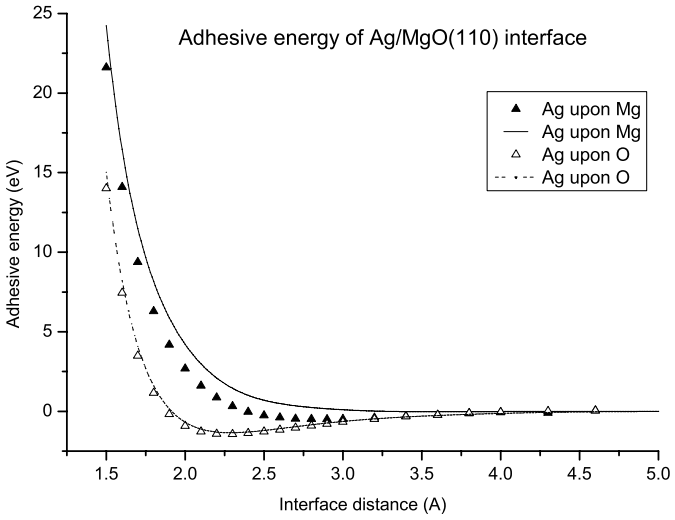

Figure 8. Adhesive energy curves from *ab initio* calculation and summation of potentials for Ag/MgO(110). Triangles represent the *ab initio* results, and curves represent the summation of potentials.

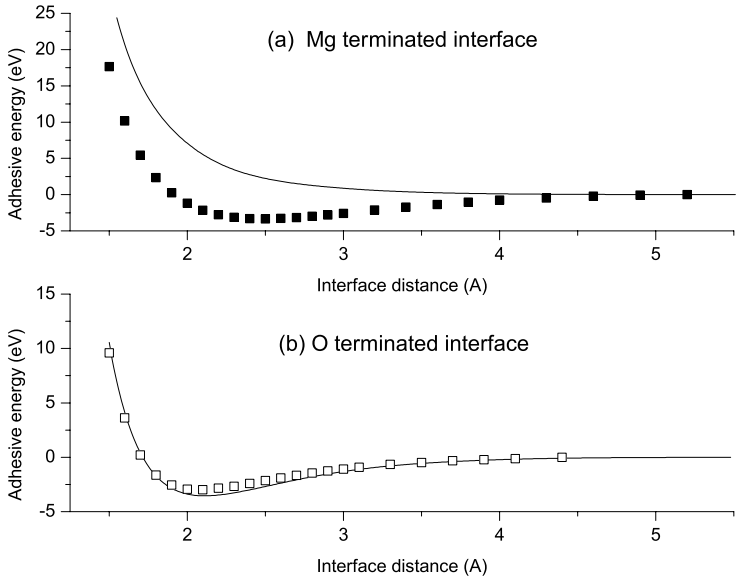

Figure 9. Adhesive energy curves from *ab initio* calculation and summation of potentials for Ag/MgO(111). (a) Mg terminated interface. (b) O terminated interface. Squares represent the *ab initio* results, and curves represent the summation of potentials.

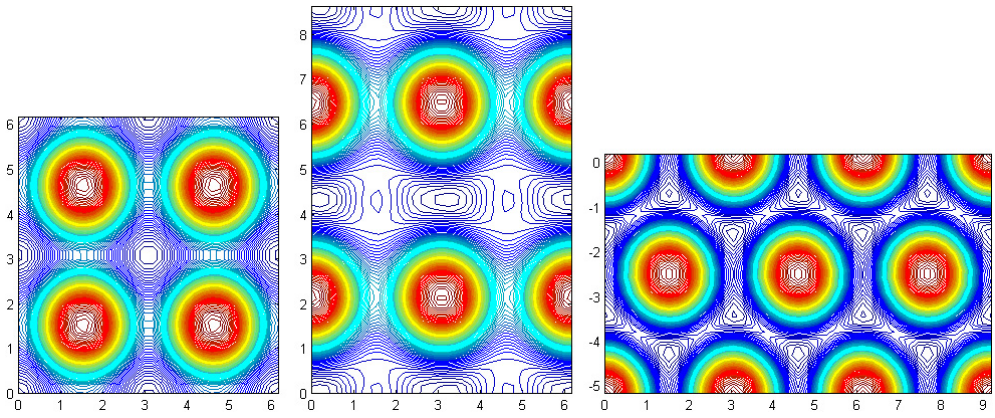

Figure 10. Logarithm contour of the charge density for the Ag/MgO interface. Left: Ag/MgO(001). Middle: Ag/MgO(110). Right: Ag/MgO(111).

(This figure is in colour only in the electronic version)

4. Conclusion

In this work, a Mobius inversion method to obtain interfacial pair potentials from *ab initio* energy curves has been introduced. There are several advantages with this new general method. First, a concise formula is given, second, the original *ab initio* energy curves can be exactly reproduced for most low energy interfacial states. Through this inversion procedure, the atomistic simulation can represent *ab initio* computation to a large extent. Note that the present Mobius inversion method is also applicable to metal/metal and metal/semiconductor interfaces.

There are also some limits for our work. First, we find that the potentials obtained from the Ag/MgO(001) interface cannot reproduce the energy curves of Ag/MgO(110) and Ag/MgO(111) in high energy states. This reveals that the transferability of these potentials is limited. Considering this question, complexity behind pair potentials is needed, such as the three-body potentials across the interface. Second, some ignored features in this work such as charge transfer should be considered in our future study. Also, the detail of the convergence and numerical stability of the inversion procedure will be presented in another work.

Acknowledgments

The authors gratefully acknowledge helpful discussions with Dr Kohyama at the Advanced Institute of Industrial Science and Technology and Dr Woo at Hong Kong Polytechnic University. This work is partly supported by the National Science Foundation of China under grant 10274035 and by the 973 Project in China under grant G2000067101.

References

[1] Guenard P, Renaud G and Villette B 1996 Structure, translational state and morphology of the Ag/MgO(001) interface during its formation *Physica* B **221** 205
[2] Renaund G, Guenard P and Barbier A 1998 Misfit dislocation network at the Ag/MgO (001) interface: a grazing-incidence x-ray-scattering study *Phys. Rev.* B **58** 7310
[3] Robach O, Renaud G and Barbier A 1998 Very-high-quality MgO(001) surfaces: roughness, rumpling and relaxation *Surf. Sci.* **401** 227
Robach O, Renaud G and Barbier A 1999 Structure and morphology of the Ag/MgO(001) interface during *in situ* growth at room temperature *Phys. Rev.* B **60** 5858
[4] Lu P and Cosandey F 1992 Electron microscopy studies of metal/MgO interfaces *Ultramicroscopy* **40** 271
[5] Trampert A *et al* 1992 High resolution transmission electron microscopy studies of the Ag/MgO interface *Acta Metall. Mater.* **40** S227
[6] Epicier T and Esnouf C 1994 Benefits of HREM for the study of metal–ceramic interfaces *J. Physique* III **4** 1811
[7] Pippel E *et al* 2000 Evidence of oxygen segregation at Ag/MgO interfaces *Acta Mater.* **48** 2571
[8] Hosson J and Kooi B 2001 Metal/ceramic interfaces: a microscopic analysis *Surf. Interface Anal.* **31** 637
[9] Smith J R, Hong T and Srolovitz D J 1994 Metal–ceramic adhesion and the Harris functional *Phys. Rev. Lett.* **72** 4021
[10] Finnis M W, Kruse C and Schonberger U 1995 *Ab initio* calculations of metal/ceramic interfaces: What have we learned, what can we learn? *Nanostruct. Mater.* **6** 145
[11] Goniakowski J 1999 Transition metals on the MgO(100) surface: evolution of adsorption characteristics along the 4d series *Phys. Rev.* B **59** 11047
[12] Snyder J A *et al* 2000 LDA and GGA calculations of alkali metal adsorption at the (001) surface of MgO *J. Chem. Phys.* **112** 3014
[13] Neyman K M *et al* 2004 Adsorption of d-metal atoms on the regular MgO(001) surface: density functional study of cluster models embedded in an elastic polarizable environment *Appl. Phys.* A **78** 823
[14] Finnis M W 1992 Metal–ceramic cohesion an the image interaction *Acta Metall. Mater.* **40** S25
[15] Duffy D M, Harding J H and Stoneham A M 1992 Atomistic modeling of the metal/oxide interface with image interactions *Acta. Metall. Mater.* **40** S11
Duffy D M, Harding J H and Stoneham A M 1993 Atomistic modeling of the metal/oxide interface with image interactions *Phil. Mag.* A **67** 865
[16] Purton J, Parker S C and Bullett D W 1997 Computer modeling of metal–oxide interfaces *J. Phys.: Condens. Matter* **9** 5709
[17] Purton J A *et al* 1999 Comparison of atomistic simulations and pseudopotential calculations of the MgO{100}/Ag{100} and MgO{110}/Ag{110} interfaces *J. Chem. Phys.* **110** 8090
[18] Bazant M Z and Kaxiras E 1996 Modeling of covalent bonding in solids by inversion of cohesive energy curves *Phys. Rev. Lett.* **77** 4370
[19] Bazant M Z, Kaxiras E and Justo J F 1997 Environment-dependent interatomic potential for bulk silicon *Phys. Rev.* B **56** 8542

[20] Justo J F *et al* 1998 Interatomic potential for silicon defects and disordered phases *Phys. Rev.* B **58** 2539
[21] Endou A *et al* 2000 Potential energy surface and dynamics of Pd/MgO(001) system, as investigated by periodic density functional calculations and classical molecular dynamics simulations *J. Appl. Phys.* **39** 4255
[22] Yao Y G and Zhang Y 1999 *Ab initio* pair potentials at metal–ceramic interfaces *Phys. Lett.* A **256** 391
[23] García-Moliner F and Velasco V 1992 *Theory of Single and Multiple Interfaces* (Singapore: World Scientific)
[24] Quintanar C, Baquero R, Velasco V R and García-Moliner F 1991 *Rev. Mex. Fís.* **37** 503
[25] Chen N X 1990 Modified Mobius inverse formula and its applications in Physics *Phys. Rev. Lett.* **64** 1193
[26] Chen N X and Rong E Q 1998 Unified solution of the inverse capacity problem *Phys. Rev.* E **57** 1302
[27] Zhang S and Chen N X 2003 Molecular dynamics simulations for high-pressure induced B1–B2 transition in NaCl by Mobius pair potentials *Modelling Simul. Mater. Sci. Eng.* **11** 331
Zhang S and Chen N X 2003 Study on the high-pressure properties of KCl crystal by inversion pair potentials *Mater. Sci. Eng.* B **99** 588
Zhang S and Chen N X 2003 Determination of the B1–B2 transition path in RbCl by Mobius pair potentials *Phil. Mag.* **83** 1451
[28] Hao S Q, Chen N X and Shen J 2002 The space group of $Nd_3Fe_{29-x}Ti_x$: $A2/m$ or $P2_1/c$ *Phys. Status Solidi* b **234** 487
[29] Zhang S and Chen N X 2005 Lattice inversion for interatomic potentials in AlN, GaN and InN *Chem. Phys.* at press
[30] Dmitriev S V *et al* 2003 Coherency of copper/sapphire interface studied by atomistic simulation and geometrical analysis *Surf. Sci.* **542** 45
[31] Dmitriev S V *et al* 2004 Atomistic structure of the $Cu(111)/a$-$Al_2O_3(0001)$ interface in terms of interatomic potentials fitted to *ab initio* results *Acta Mater.* **52** 1959
[32] Accelrys Inc. *CASTEP Users Guide*
[33] Milman V *et al* 2000 *Int. J. Quantum Chem.* **77** 895
[34] Monkhorst H J and Pack J D 1976 Special points for Brillouin-zone integrations *Phys. Rev.* B **13** 5188
[35] Macdonald A H 1978 Comment on special points for Brillouin-zone integrations *Phys. Rev.* B **18** 5897